J. Cell. Mol. Med. Vol 12, No 3, 2008 pp. 962-974

# $Na^+$-independent $Mg^{2+}$ transport sensitive to 2-aminoethoxydiphenyl borate (2-APB) in vascular smooth muscle cells: involvement of TRPM-like channels

Yukihisa Hamaguchi [a, b], Tatsuaki Matsubara [e], Tetsuya Amano [a], Tadayuki Uetani [a], Haruhiko Asano [c], Takashi Iwamoto [c], Koichi Furukawa [d], Toyoaki Murohara [a], Shinsuke Nakayama [b, *]

[a] Department of Cardiology, Nagoya University Graduate School of Medicine, Nagoya, Japan
[b] Department of Cell Physiology, Nagoya University Graduate School of Medicine, Nagoya, Japan
[c] Department of Biomedical Sciences, College of Life and Health Sciences, Chubu University, Aichi, Japan
[d] Department of Biochemistry II, Nagoya University Graduate School of Medicine, Nagoya, Japan
[e] Department of Internal Medicine, Aichi-Gakuin University School of Dentistry, Nagoya, Japan

Received: July 19, 2007; Accepted: October 24, 2007

## Abstract

Magnesium is associated with several important cardiovascular diseases. There is an accumulating body of evidence verifying the important roles of $Mg^{2+}$-permeable channels. In the present study, we estimated the intracellular free $Mg^{2+}$ concentration ($[Mg^{2+}]_i$) using $^{31}$P-nuclear magnetic resonance ($^{31}$P-NMR) in porcine carotid arteries. $pH_i$ and intracellular phosphorus compounds were simultaneously monitored. Removal of extracellular divalent cations ($Ca^{2+}$ and $Mg^{2+}$) in the absence of $Na^+$ caused a gradual decrease in $[Mg^{2+}]_i$ to ~60% of the control value after 125 min. On the other hand, the simultaneous removal of extracellular $Ca^{2+}$ and $Na^+$ in the presence of $Mg^{2+}$ gradually increased $[Mg^{2+}]_i$ in an extracellular $Mg^{2+}$-dependent manner. 2-aminoethoxydiphenyl borate (2-APB) attenuated both $[Mg^{2+}]_i$ load and depletion caused under $Na^+$- and $Ca^{2+}$-free conditions. Neither $[ATP]_i$ nor $pH_i$ correlated with changes in $[Mg^{2+}]_i$. RT-PCR detected transcripts of both TRPM6 and TRPM7, although TRPM7 was predominant. In conclusion, the results suggest the presence of $Mg^{2+}$-permeable channels of TRPM family that contribute to $Mg^{2+}$ homeostasis in vascular smooth muscle cells. The low, basal $[Mg^{2+}]_i$ level in vascular smooth muscle cells is attributable to the relatively low activity of this $Mg^{2+}$ entry pathway.

**Keywords:** magnesium • vascular smooth muscle • 2-aminoethoxydiphenyl borate • ATP • NMR

## Introduction

From both clinical and epidemiologic aspects, $Mg^{2+}$-deficiency is related to cardiovascular diseases [1–3]. More $Mg^{2+}$ intake is recommended to prevent arteriosclerosis and hypertension. It is important, however, to point out that the serum $Mg^{2+}$ level does not reflect $Mg^{2+}$-deficiency of the entire body [4]. Cellular $Mg^{2+}$-deficiency is caused by a malfunction of $Mg^{2+}$ transporters across the plasma membrane, as well as a fall in the extracellular $Mg^{2+}$ concentration. It is therefore of great interest to investigate mechanisms driving $Mg^{2+}$ transport into the cell, especially into vascular smooth muscle cells.

*Correspondence to: S. NAKAYAMA,
Department of Cell Physiology, Nagoya University Graduate School of Medicine, Nagoya 466-8550, Japan.
Tel.: +81 52 744 2045
Fax: +81 52 744 2048
E-mail: h44673a@nucc.cc.nagoya-u.ac.jp

doi: 10.1111/j.1582-4934.2007.00157.x

$[Mg^{2+}]_i$ is believed to be regulated by two transmembrane $Mg^{2+}$ pathways: the $Na^+$–$Mg^{2+}$ exchange driven by the $Na^+$-gradient, and the $Na^+$-independent 'passive' $Mg^{2+}$ transport *via* $Mg^{2+}$-permeable channels [5–8]. Since the molecular identification of the latter $Mg^{2+}$ pathway, such as melastatin-type transient receptor potential (TRPM) homologue channels, there has been an accumulating body of evidence for the crucial role that this pathway plays in $Mg^{2+}$ homeostasis [9–11]. Also, TRPM homologue channels are bifunctional proteins, which contain a kinase domain in the C-terminus.

$[Mg^{2+}]_i$ is known to change slowly, and thereby act as a chronic regulator. In addition, changes in the intracellular milieu, such as the intracellular pH ($pH_i$) and $[ATP]_i$ can affect $[Mg^{2+}]_i$ regulation. However, the importance of TRPM homologues in $[Mg^{2+}]_i$ regulation during relatively short durations has been assessed using fluorescent $Mg^{2+}$ indicators. In the present study, we thus utilized $^{31}$P-NMR to estimate slow changes in $[Mg^{2+}]_i$ over several hours in carotid arteries, which are now frequently used as a model to evaluate arteriosclerotic changes, and assessed the contribution of TRPM-like $Mg^{2+}$-permeable channels.

# Materials and methods

## Preparation

Porcine carotid arteries were collected at an abattoir. The arteries were stripped of fat and connective tissue, and cut into segments of approximately 30 mm in length. The lumen was exposed by cutting the artery segments into two strips along the longitudinal direction. The endothelium was removed by scratching with a cotton-tipped stick. The resultant pig carotid artery strips (~2 g wet weight) were mounted in a sample tube of 10 mm in diameter. This study was approved by the institutional committee of animal experiments.

## $^{31}$P-NMR

The methods employed for the $^{31}$P-NMR measurements were essentially the same as those previously described [12]. NMR spectrometers (GSX270W: JEOL, Tokyo, Japan; UNITY-500plus: Varian, Tokyo, Japan) were operated at 109.4 and 202.3 MHz, respectively. The temperature of the sample was maintained at 32°C. Radio frequency pulses corresponding to a flip angle of 30 were applied every 0.6 sec. $^{31}$P-NMR spectra were obtained by accumulating 2500 signals (free induction decays) over 25 min. Before Fourier transformation, a broadening factor of 20 Hz was applied to enhance the signal-to-noise ratio. Spectral peak resonances (frequencies) were measured relative to that of phosphocreatine (PCr) in p.p.m.

Control spectra were acquired in the absence of $Ca^{2+}$. Then, experiments were carried out in the absence of extracellular $Na^+$ to rule out the contribution of $Na^+$-coupled $Mg^{2+}$ transport, that is, $Na^+$–$Mg^{2+}$ exchange. Six major peaks were observed (Fig. 1): phosphomonoesters (PME), inorganic phosphate ($P_i$), PCr and the γ-, α- and β-phosphorus atoms of ATP (γ-, α- and β-ATP).

Concentrations of phosphorus compounds were estimated by integrating the peak areas (Scion image; Scion Corp., Fredrick, MA, U.S.A.) and by correcting with their saturation factors ($P_i$, 1.60; PCr, 1.36; β-ATP, 1.07).

## Estimation of $[Mg^{2+}]_i$ and $pH_i$

Intracellular pH ($pH_i$) was estimated from the chemical shift observed for the $P_i$ peak ($\delta_{o(Pi)}$), using a Henderson–Hasselbalch type equation:

$$pH_i = pK_a + \log_{10}[(\delta_{o(Pi)} - \delta_{p(Pi)})/(\delta_{d(Pi)} - \delta_{o(Pi)})], \quad \text{Eq(1)}$$

where $pK_a$ is the negative logarithm of the dissociation constant of $P_i$ (= 6.70), and $\delta_{p(Pi)}$ and $\delta_{d(Pi)}$ are the chemical shifts for $H_2PO_4^-$ (= 3.15 p.p.m.) and $HPO_4^{2-}$ (= 5.72 p.p.m.), respectively. The $pH_i$ value was used to correct the $[Mg^{2+}]_i$ estimation.

$Mg^{2+}$ usually binds to ATP as a 1 to 1 complex. $[Mg^{2+}]_i$ was thus estimated from the chemical shift observed for the β-ATP peak ($\delta_{o\beta}$) using the following equation [13,14]:

$$[Mg^{2+}]_i = K_D\text{“MgATP”} (\delta_{o\beta} - \delta_{f\beta}) / (\delta_{b\beta} - \delta_{o\beta}), \text{ Eq(2)}$$

where $\delta_{f\beta}$ and $\delta_{b\beta}$ are the chemical shifts of metal-free and $Mg^{2+}$-bound forms of β-ATP, respectively. We have previously shown that $K_D$“MgATP”, $\delta_{f\beta}$ and $\delta_{b\beta}$ can be described as functions of pH [15] (See, Supplementary Material S1: Details of estimation procedures). $K_D$“MgATP”($pH_i$) was derived from quadratic pH-functions for $K_D$“MgATP” at 25 and 37°C [16], using the van't Hoff isochore. The pH–functions of $\delta_{f\beta}$ and $\delta_{b\beta}$ were constructed by fitting the data points of model solutions with sigmoid curves [17]. Thus, Eq(2) can be rewritten as:

$$[Mg^{2+}]_i = K_D\text{“MgATP”}(pH_i) (\delta o\beta - \delta_{f\beta}(pH_i)) / (\delta_{b\beta(pHi)} - \delta_{o\beta}). \quad \text{Eq(3)}$$

In Table 2, $[Mg^{2+}]_i$ and $pH_i$ values were also estimated from the chemical shifts of β- and γ-ATP [12,17]. For the

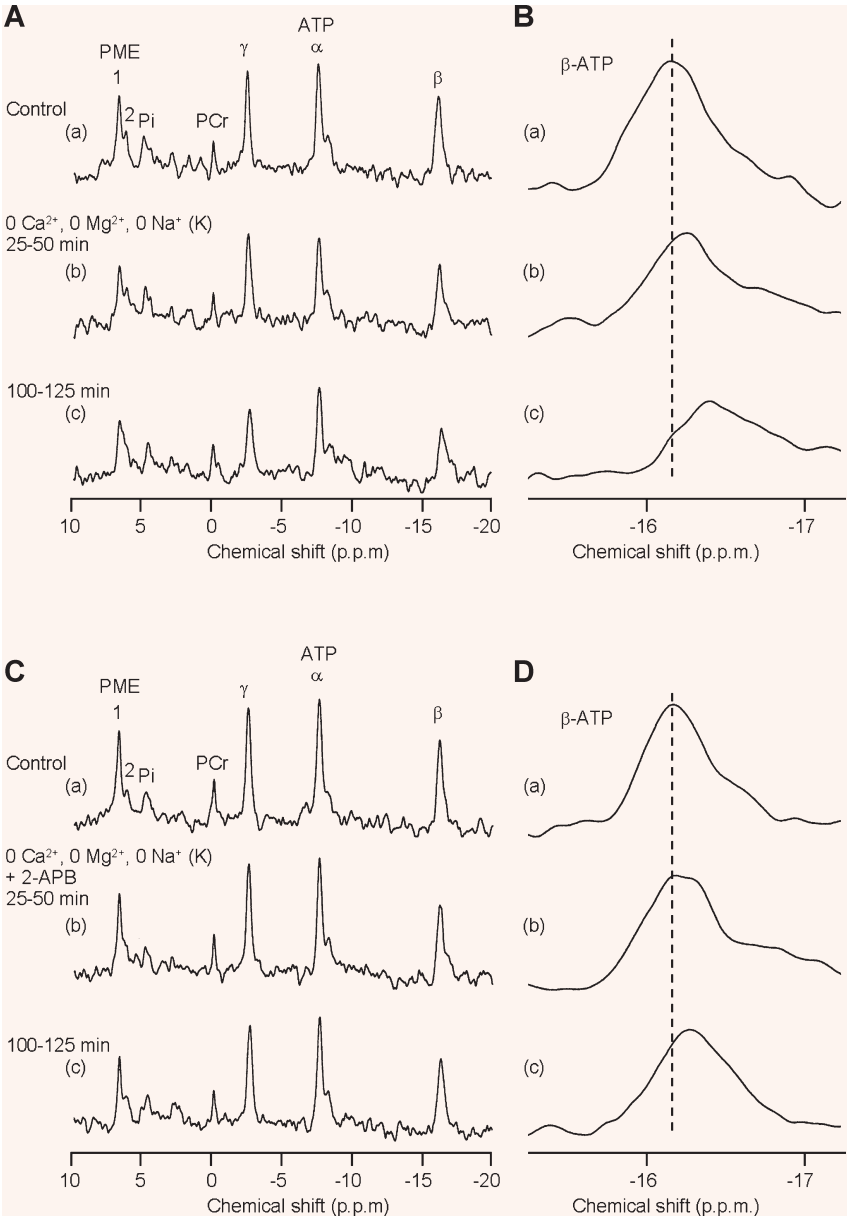


**Fig. 1** Changes in the $^{31}$P-NMR spectrum during exposures to a divalent-cation-free, $Na^+$-free solution. After acquiring the control spectrum in a $Ca^{2+}$-free solution (a), extracellular $Mg^{2+}$ and $Na^+$ were simultaneously removed (0 $Ca^{2+}$, 0 $Mg^{2+}$, 0 $Na^+$: $K^+$ substitution) for 125 min. The spectra (b) and (c) were obtained during 25–50 min and 100–125 min periods, respectively. Each spectrum was obtained with 2500 signals accumulated over 25 min. The whole spectrum is shown in (**A**), and the β-ATP peaks are shown expanded in (**B**). The vertical line indicates the initial chemical shift of the β-ATP peak. The explanations are the same for the spectra in (**C**) and (**D**), but the divalent cation-free, $Na^+$-free solution (0 $Ca^{2+}$, 0 $Mg^{2+}$, 0 $Na^+$: $K^+$ substitution) contained 150 μM 2-APB.

chemical shift of γ-ATP, an equation analogous to Eq(3) can be written:

$$[Mg^{2+}]_i = K_D\text{“MgATP”}(pH_i)\ (\delta_O\gamma - \delta_{f\gamma}(pH_i)) / (\delta_{b\gamma}(pH_i) - \delta_O\gamma), \quad \text{Eq(4)}$$

$\delta_{f\gamma}$ and $\delta_{b\gamma}$ are the chemical shifts of metal-free and $Mg^{2+}$-bound forms of γ-ATP, respectively, and these parameters are also expressed as pH-functions. $[Mg^{2+}]_i$ and $pH_i$ were estimated by solving the Eq(3) and Eq(4) simultaneously.

Similar to the effect of $Mg^{2+}$, $Ca^{2+}$-binding to ATP changes the chemical shifts of the ATP peaks. However, basal $[Ca^{2+}]_i$ is maintained at ~100 nM in smooth muscle cells under physiological conditions. Furthermore, experiments in the present study were carried out mainly under $Ca^{2+}$-free conditions. Therefore, the effect of $Ca^{2+}$-binding to ATP is considered negligible.

## Solutions and chemicals

The extracellular solution used for the ‘normal’ solution had the following composition in mM: NaCl, 137.9; $KHCO_3$ 5.9; $CaCl_2$ 2.4; $MgCl_2$ 1.2; glucose 11.8; HEPES 5 (pH adjusted

**Table 1** PCR primers. PCR primers for porcine sample were designed by using the conserved sequences in humans and mice

| Clones | Primer Sequence (+): Sense, (-): Antisense | Primer site (in human clones) | Accession No (human) (mouse) |
|---|---|---|---|
| TRPM2 | (+):5'-TTC CAG GAG ATG TTT GAG AC-3' | 1604-1938 | NM_003307 |
| | (-):5'-TCA GGC TTG TTG GAG ATG AG-3' | | NM_138301 |
| TRPM4 | (+):5'-GTG GGA GGG ACT GGA ATT GA-3' | 863-1263 | NM_017636 |
| | (-):5'-AGC TCA TCC AGG TAG GCT GA-3' | | NM_175130 |
| TRPM6 | (+):5'-TGT TGG TGG AGA TGC AGC C-3' | 2862-3174 | NM_017662 |
| | (-):5'-CCT GCA TGT TGA TTC ACA GC-3' | | NM_153417 |
| TRPM7 | (+):5'-GAT GCC CTC AAA GAA CAT GC-3' | 794-1269 | NM_017672 |
| | (-):5'-GGC TCT GCT GCA TCA GGA AG-3' | | NM_021450 |

to 7.4–7.5 at 32°C). The ionic composition was modified iso-osmotically. Also, divalent cation-free solutions contained 1 mM EDTA. The solutions used for $^{31}$P-NMR measurements were normally aerated with 95% $O_2$/5%$CO_2$. 2-aminoethoxydiphenyl borate (2-APB) was purchased from Calbiochem (San Diego, CA, USA).

## RT-PCR

The procedures for RT-PCR were essentially the same as previously described [18]. Total RNA was extracted from porcine carotid arteries. After treatment with RQ1 DNase (Promega, Madison, WI, USA), the total RNA was subjected to an RT (reverse-transcription) reaction. RT was performed using a random hexamer (12 pmol/reaction) and Moloney murine leukemia virus (MMLV) reverse transcriptase 5 (100 U/reaction) according to the manufacture's instructions (Gibco-BRL, Rockville MD, U.S.A.). The cycling condition was 3 min of initial denaturation at 95°C followed by 35 cycles of 95°C for 30 sec, 54°C for 30 sec and 72°C for 35 sec. The RT sample was then used as a template for the PCR reaction. The amplicons (5 μl were run on a 2.5% agarose gel and stained with ethidium bromide. Because the cDNA sequences for porcine TRP (transient receptor potential) homologue cation channels have not been published, the PCR primers were designed by using the conserved sequences in humans and mice. The primers used are listed in Table 1.

## Statistics

Numerical data are expressed as the mean (S.D. Differences between groups with different experimental protocols were evaluated by use of ANOVA for repeated measures. When a significant difference was identified between the groups ($P$<0.05), individual comparisons at the same time point were performed using an unpaired t-test.

# Results

## Depletion of $[Mg^{2+}]_i$ *via* $Na^+$-independent $Mg^{2+}$ pathways

$^{31}$P-NMR was used to continuously measure phosphorus compounds in porcine carotid artery smooth muscle (Fig. 1). In this study, we mainly estimated $[Mg^{2+}]_i$ from the chemical shift of the β-ATP peak, and correction was made by $pH_i$ estimated from the chemical shift of the $P_i$ peak.

During exposure to a divalent cation-free solution (*i.e.* 0 $Ca^{2+}$, 0 $Mg^{2+}$), $[Mg^{2+}]_i$ decreased from from 0.74±0.11 to 0.49±0.08 mM (n = 7; Fig. 2A, ■) after 125 min, while $pH_i$ did not change significantly (Fig. 2B, ●). Essentially the same decrease in $[Mg^{2+}]_i$ (from 0.75±0.09 to 0.46±0.05 mM; n = 7; Fig. 2A, □) was observed in the absence of $Na^+$, suggesting that $Mg^{2+}$-permeable channels make a major contribution to the changes in $[Mg^{2+}]_i$ under divalent cation-free conditions. On the other hand, $pH_i$ decreased from 7.09 ± 0.05 to 6.92 ± 0.05 (n = 7) after 125 min in the absence of $Na^+$ (Fig. 2B, ○), presumably due to the inhibition of $Na^+$-coupled $pH_i$ regulatory mechanisms, such as $Na^+$-$H^+$ exchange and $Na^+$-$HCO_3^-$ co-transport.

**Table 2** $[Mg^{2+}]_i$ and $pH_i$ values estimated using two methods: (1) from the chemical shifts of β-and γ-ATP or 2) from the chemical shifts of β-ATP and $P_i$. (See Materials and methods for details). $[Mg^{2+}]_i$ and $pH_i$ values during $[Mg^{2+}]_i$ depletion were compared in A and B. In C and D, $[Mg^{2+}]_i$ and $pH_i$ values were during the elevation of $[Mg^{2+}]_i$. Single (*) and double asterisks (**) indicate $P<0.05$ and $P<0.01$ *versus* control, respectively.

(A) Exposure to a divalent cation- and $Na^+$-free solution (n = 7).

| | 1) from β- and γ-ATP | | 2) from β-ATP and $P_i$ | |
|---|---|---|---|---|
| | $[Mg^{2+}]_i$ (mM) | $pH_i$ | $[Mg^{2+}]_i$ (mM) | $pH_i$ |
| Control (0 $Ca^{2+}$) | 0.70±0.13 | 7.20±0.11 | 0.75±0.09 | 7.09±0.05 |
| 0 $Ca^{2+}$, 0 $Mg^{2+}$, 0 $Na^+$ ($K^+$) 25–50 min | 0.61±0.07** | 7.09±0.09** | 0.62±0.04** | 7.06±0.04** |
| 0 $Ca^{2+}$, 0 $Mg^{2+}$, 0 $Na^+$ ($K^+$) 100–125 min | 0.43±0.04** | 7.01±0.08** | 0.46±0.05** | 6.92±0.05** |

(B) Exposure to a divalent cation- and $Na^+$-free solution containing 2-APB (n = 7).

| | 1) from β- and γ-ATP | | 2) from β-ATP and $P_i$ | |
|---|---|---|---|---|
| | $[Mg^{2+}]_i$ (mM) | $pH_i$ | $[Mg^{2+}]_i$ (mM) | $pH_i$ |
| Control (0 $Ca^{2+}$) | 0.68±0.04 | 7.21±0.05 | 0.74±0.05 | 7.09±0.04 |
| 0 $Ca^{2+}$, 0 $Mg^{2+}$, 0 $Na^+$ ($K^+$) +150μM 2-APB 25–50 min | 0.65±0.08* | 7.09±0.08** | 0.68±0.07* | 7.03±0.04** |
| 0 $Ca^{2+}$, 0 $Mg^{2+}$, 0 $Na^+$ ($K^+$) +150μM 2-APB 100–125 min | 0.60±0.12** | 7.00±0.11** | 0.62±0.08** | 6.94±0.05** |

(C) Exposure to a $Ca^{2+}$- and $Na^+$-free, high $Mg^{2+}$ (6.0 mM) solutions (n = 7).

| | 1) from β- and γ-ATP | | 2) from β-ATP and $P_i$ | |
|---|---|---|---|---|
| | $[Mg^{2+}]_i$ (mM) | $pH_i$ | $[Mg^{2+}]_i$ (mM) | $pH_i$ |
| Control (0 $Ca^{2+}$) | 0.72±0.10 | 7.20±0.09 | 0.78±0.08 | 7.08±0.12 |
| 0 $Ca^{2+}$, 6.0 $Mg^{2+}$, 0 $Na^+$ ($K^+$) 25–50 min | 1.11±0.28** | 7.12±0.10** | 1.18±0.28** | 7.03±0.05** |
| 0 $Ca^{2+}$, 6.0 $Mg^{2+}$, 0 $Na^+$ ($K^+$) 100–125 min | 1.63±0.23** | 6.99±0.11** | 1.79±0.18** | 6.92±0.04** |

(D) Exposure to a $Ca^{2+}$- and $Na^+$-free, high $Mg^{2+}$ (6.0 mM) solution containing 2-APB (n = 6).

| | 1) from β- and γ-ATP | | 2) from β-ATP and $P_i$ | |
|---|---|---|---|---|
| | $[Mg^{2+}]_i$ (mM) | $pH_i$ | $[Mg^{2+}]_i$ (mM) | $pH_i$ |
| Control (0 $Ca^{2+}$) | 0.70±0.09 | 7.20±0.11 | 0.75±0.04 | 7.10±0.03 |
| 0 $Ca^{2+}$, 6.0 $Mg^{2+}$, 0 $Na^+$ ($K^+$) +150μM 2-APB 25–50 min | 0.91±0.10** | 7.06±0.07** | 0.93±0.06** | 7.02±0.02** |
| 0 $Ca^{2+}$, 6.0 $Mg^{2+}$, 0 $Na^+$ ($K^+$) +150μM 2-APB 100–125 min | 1.10±0.08** | 6.99±0.04** | 1.14±0.08** | 6.95±0.03** |

## Effects of 2-APB in $Na^+$-independent depletion of $[Mg^{2+}]_i$

2-APB is known to block TRPM7 [11]. To substantiate the involvement of analogous $Mg^{2+}$-permeable channels in vascular muscle cells, the effect of 2-APB was examined (Fig. 1C and D). As shown in Figure 3, application of 150 μM 2-APB to the divalent cation- and $Na^+$-free solution significantly attenuated the depletion of $[Mg^{2+}]_i$ (from 0.74 ± 0.05 to 0.62 ± 0.08 mM after 125 min; Fig. 3A, ■). This inhibitory effect of 2-APB was concentration-dependent (Fig. 3C). The decrease in $[Mg^{2+}]_i$ after 125 min was –0.27 ± 0.11 mM at 15 μM (n = 5), (0.22 ± 0.07 mM at 50 μM (n = 5) and –0.12±0.08 mM at 150 μM (n = 7). On the other hand, this drug had little effect on the changes in $pH_i$ (unpaired t-test, $P$ >0.05, n = 7; Fig. 3B, ●).

## Increase in $[Mg^{2+}]_i$ *via* $Na^+$-independent $Mg^{2+}$ pathways

Next, to demonstrate the increase in $[Mg^{2+}]_i$ *via* transmembrane $Mg^{2+}$-permeable channels, the effect of $Na^+$ removal was examined in the presence of $Mg^{2+}$ (Supplementary Fig. S1, A). Extracellular $Ca^{2+}$ was again removed to potentiate $Mg^{2+}$ transport, *i.e.* to reduce competition between divalent cations at the channel pore.

Changes in $[Mg^{2+}]_i$ and $pH_i$ during exposure to $Ca^{2+}$- and $Na^+$-free solutions are shown in Figures 4A and B, respectively. In the presence of 1.2 mM $Mg^{2+}$ (the 'normal' $Mg^{2+}$ concentration in extracellular medium), $[Mg^{2+}]_i$ increased from 0.73±0.07 to 1.01±0.09 mM after 125 min (■; $n$ = 5; $P$<0.01). When the concentration of extracellular $Mg^{2+}$ was increased to 6.0 mM, $[Mg^{2+}]_i$ increased from 0.78±0.08 to 1.79 ± 0.18 mM after 125 min (□; $n$ = 7; $P$<0.01). The $[Mg^{2+}]_i$ rise was clearly enhanced by raising the extracellular $Mg^{2+}$ concentration (unpaired t-test, $P$<0.01).

## Effects of 2-APB on the increase in $[Mg^{2+}]_i$

To assess whether the same $Mg^{2+}$-permeable channels contributed to the inward and outward transport of $Mg^{2+}$ under $Na^+$-free conditions, we examined the effect of 2-APB in the presence of $Mg^{2+}$. 2-APB (150 μM) was applied to a $Ca^{2+}$- and $Na^+$-free

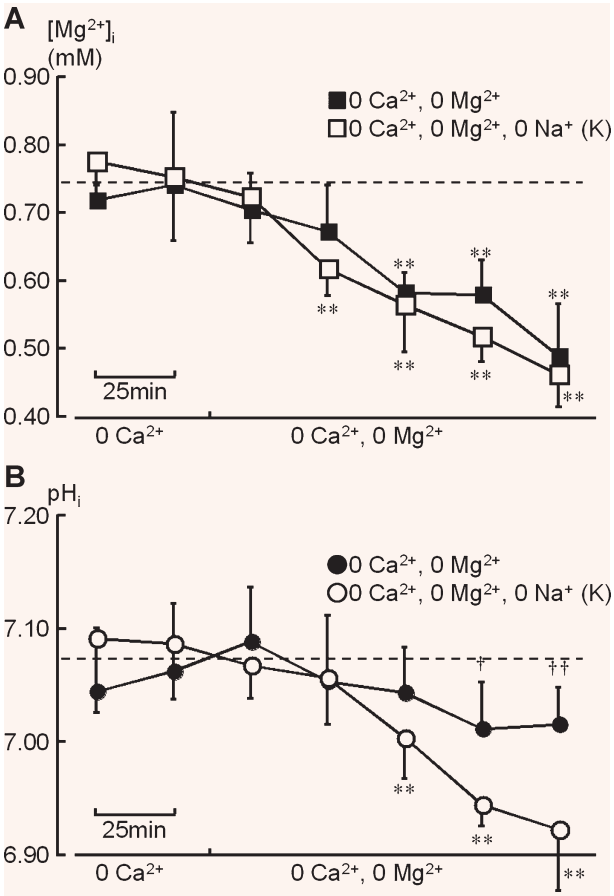


**Fig. 2** Time course of changes in $[Mg^{2+}]_i$ (**A**: squares) and $pH_i$ (**B**: circles) during exposure to divalent cation-free solutions. After control measurements in a $Ca^{2+}$-free solution (control), extracellular $Mg^{2+}$ was also removed for 125 min. Each point was obtained from the accumulation of NMR signals over 25 min. The open (□, ○) and filled symbols (■, ●) represent the data obtained under exposures to $Na^+$-free (0 $Ca^{2+}$, 0 $Mg^{2+}$, 0 $Na^+$: $K^+$ substitution; n=7) and $Na^+$-containing solutions (0 $Ca^{2+}$, 0 $Mg^{2+}$; n = 7), respectively. The spectra shown in Fig. 1A and B correspond to this $Na^+$-free experiment. The dotted lines indicate the mean value of $[Mg^{2+}]_i$ and $pH_i$ before exposure to the divalent cation-free solutions ($n$ = 14 for all preparations shown in this figure). Vertical bars represent S.D. values. Asterisks indicate statistically significant differences compared to the $[Mg^{2+}]_i$ and $pH_i$ values before removal of extracellular $Mg^{2+}$ (*, $P$<0.05; **, $P$<0.01). Crosses on filled symbols, in the presence of $Na^+$, indicate statistically significant differences compared to the open symbols, in the absence of $Na^+$, at the same time point (†, $P$<0.05; ††, $P$<0.01).

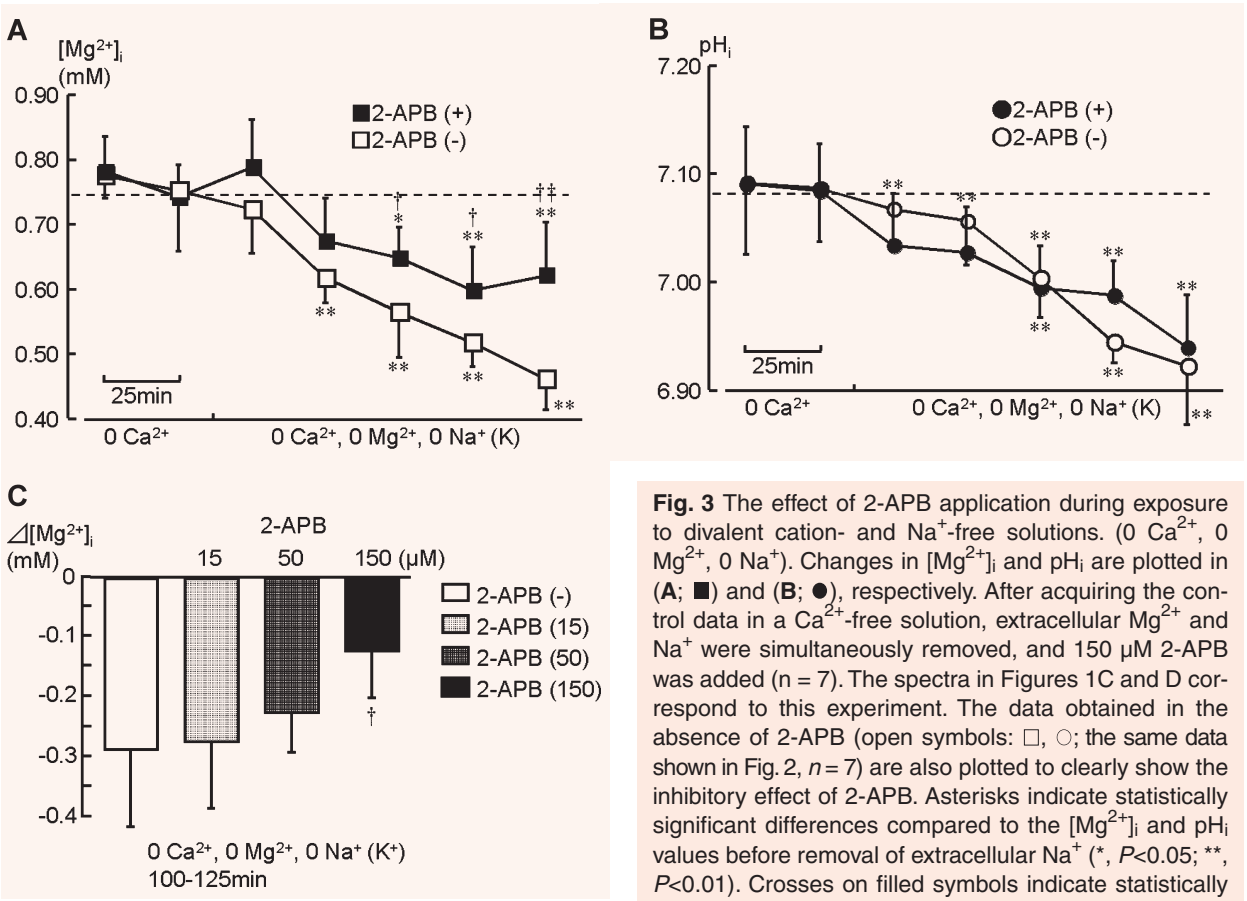


**Fig. 3** The effect of 2-APB application during exposure to divalent cation- and $Na^+$-free solutions. (0 $Ca^{2+}$, 0 $Mg^{2+}$, 0 $Na^+$). Changes in $[Mg^{2+}]_i$ and $pH_i$ are plotted in (**A**; ■) and (**B**; ●), respectively. After acquiring the control data in a $Ca^{2+}$-free solution, extracellular $Mg^{2+}$ and $Na^+$ were simultaneously removed, and 150 μM 2-APB was added (n = 7). The spectra in Figures 1C and D correspond to this experiment. The data obtained in the absence of 2-APB (open symbols: □, ○; the same data shown in Fig. 2, $n = 7$) are also plotted to clearly show the inhibitory effect of 2-APB. Asterisks indicate statistically significant differences compared to the $[Mg^{2+}]_i$ and $pH_i$ values before removal of extracellular $Na^+$ (*, $P<0.05$; **, $P<0.01$). Crosses on filled symbols indicate statistically significant differences compared to the open symbols at the same time point (†, $P<0.05$; ††, $P<0.01$). Bar graphs in (**C**) indicate effects of 15, 50 and 150 μM 2-APB during 125–150 min ($n = 7$ in (–) and 150 μM 2-APB; $n = 5$ in 15 and 50 μM 2-APB).

solution containing 6.0 mM $Mg^{2+}$ (Supplementary Fig. S1, B). After 125 min, $[Mg^{2+}]_i$ increased from 0.75±0.04 to 1.14±0.08 mM (Fig. 5A, ■; n = 7; $P<0.01$), but this increase in $[Mg^{2+}]_i$ was significantly smaller than without 2-APB (unpaired t-test, $P<0.01$). On the other hand, $pH_i$ with and without 2-APB, was comparable throughout experiments (not shown).

A gradual, and slow increase in $[Mg^{2+}]_i$ was caused by substituting extracellular $Na^+$ with N-methyl-D-glucamine (NMDG), even in the presence of $Ca^{2+}$ (Fig. 5B, □; $n = 4$). Application of 150 μM 2-APB again attenuated the increase in $[Mg^{2+}]_i$ significantly (Fig. 5B, ■; $n = 4$; $P<0.01$), suggesting that TRPM7-like $Mg^{2+}$-permeable channels sensitive to 2-APB play a crucial role in $Mg^{2+}$ regulation (*i.e.* uptake) under physiological conditions, in which $Ca^{2+}$ is present. Lower concentrations (15 and 50 μM) of 2-APB only attenuated the increase in $[Mg^{2+}]_i$ slightly ($P>0.05$; Fig. 5C).

In the present experiments, $Na^+$ was frequently substituted with equimolar $K^+$. To rule out that $Na^+$–$Mg^{2+}$ exchangers coupled $Mg^{2+}$ transport with $K^+$ under $Na^+$-free conditions, we examined the effect of amiloride, which is known to inhibit a broad range of $Na^+$-coupled transporters [19], including $Na^+$–$Mg^{2+}$ exchange [12, 20]. Application of amiloride (1 mM) had little effect on the increase in $[Mg^{2+}]_i$ caused by exposure to a $Ca^{2+}$- and $Na^+$-free solution containing 6.0 mM $Mg^{2+}$ (unpaired t-test, $P>0.05$; see Supplementary Fig. S2).

## Estimation of $[Mg^{2+}]_i$ and $pH_i$ from the β and γ-ATP peaks

To confirm the changes in $[Mg^{2+}]_i$ and $pH_i$ estimated above, we used a different procedure; specifically,

the chemical shifts of β- and γ-ATP were used to solve simultaneous equations for $[Mg^{2+}]_i$ and $pH_i$ (see, Material and methods). The changes in $pH_i$, as well as $[Mg^{2+}]_i$, were comparable between the two analyses (Table 2). $[Mg^{2+}]_i$ estimated from β- and γ-ATP were slightly smaller because of the higher $pH_i$ estimated; *i.e.* the apparent dissociation constant for MgATP is smaller in a higher pH.

### High-energy phosphates

ATP is known to affect the activity of TRPM7 and to act as an important intracellular $Mg^{2+}$ buffer. Correlation analysis revealed that $[ATP]_i$ and $[Mg^{2+}]_i$ are not correlated regardless of the presence of extracellular $Mg^{2+}$ (Fig. 6). Also, $[PCr]_i$ did not change significantly throughout (Supplementary Table S1).

### RT-PCR

To confirm the transcription of genes for $Mg^{2+}$-permeable channels, RT-PCR was performed. Because the cDNA sequences for porcine TRP (transient receptor potential) homologue cation channels have not been published, the PCR primers were designed by using the conserved sequences from humans and mice. Of TRPM2, 4, 6 and 7, the TRPM7 was predominant. TRPM6 was also detectable under the same PCR condition (Fig. 7; see also Supplementary Fig. S3).

## Discussion

The present $^{31}$P-NMR measurements revealed several features of $[Mg^{2+}]_i$ modulation *via* transmembrane $Mg^{2+}$-permeable channels, including sensitivity to 2-APB. Simultaneous removal of extracellular $Mg^{2+}$ and $Ca^{2+}$ reduced $[Mg^{2+}]_i$ to approximately 60% of the control after 125 min even in the absence of $Na^+$ (Fig. 2), under which conditions $Na^+$-coupled $Mg^{2+}$ transporters *i.e.* $Na^+$–$Mg^{2+}$ exchange, do not operate. In addition, the removal of extracellular $Na^+$ in the presence of extracellular $Mg^{2+}$ increased $[Mg^{2+}]_i$ in an extracellular $Mg^{2+}$-concentration-dependent manner (Fig. 4), and this effect was enhanced by the simultaneous removal of $Ca^{2+}$. Altogether, these results suggested an important role of transmembrane $Mg^{2+}$-permeable channels in regulating $[Mg^{2+}]_i$ in vascular smooth muscle cells.

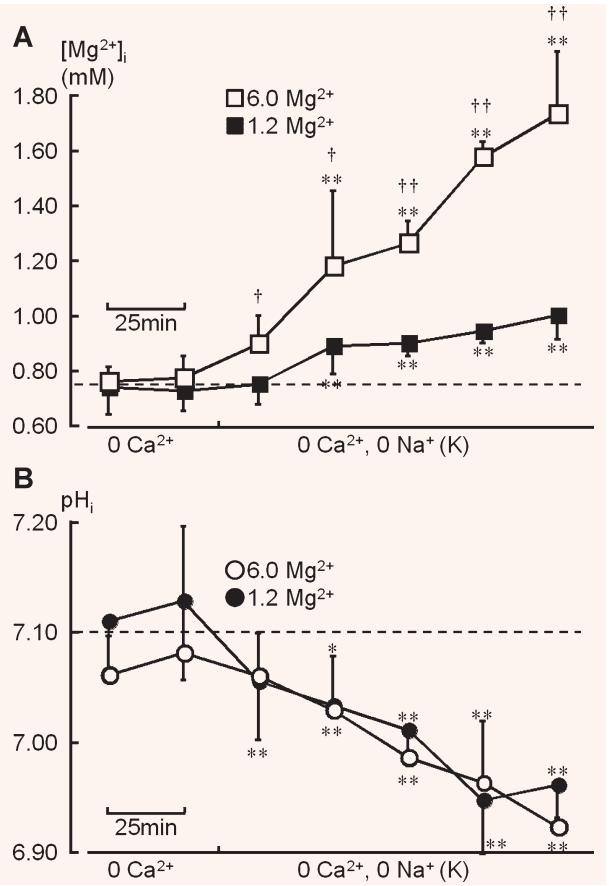


**Fig. 4** Changes in $[Mg^{2+}]_i$ (**A**) and $pH_i$ (**B**) during exposures to $Ca^{2+}$- and $Na^+$-free solutions containing $Mg^{2+}$. After the carotid artery preparations were superfused with a $Ca^{2+}$-free solution containing 1.2 mM $Mg^{2+}$, extracellular $Na^+$ was removed for 125 min (filled symbols: ■, ●). In the experiments indicated by open symbols (□, ○), extracellular $Mg^{2+}$ was increased to 6.0 mM during $Na^+$ removal. Asterisks indicate statistically significant differences compared to the $[Mg^{2+}]_i$ and $pH_i$ values before removal of extracellular $Mg^{2+}$ (*, $P$<0.05; **, $P$<0.01). Crosses on open symbols indicate statistically significant differences compared to the filled symbols at the same time point (†, $P$<0.05; ††, $P$<0.01).

As shown in Fig. 5B, the activity of $Mg^{2+}$-permeable channels are attenuated by extracellular $Ca^{2+}$, but $Mg^{2+}$ entry still occurred. In these experiments, extracellular $Na^+$ was substituted with NMDG, and

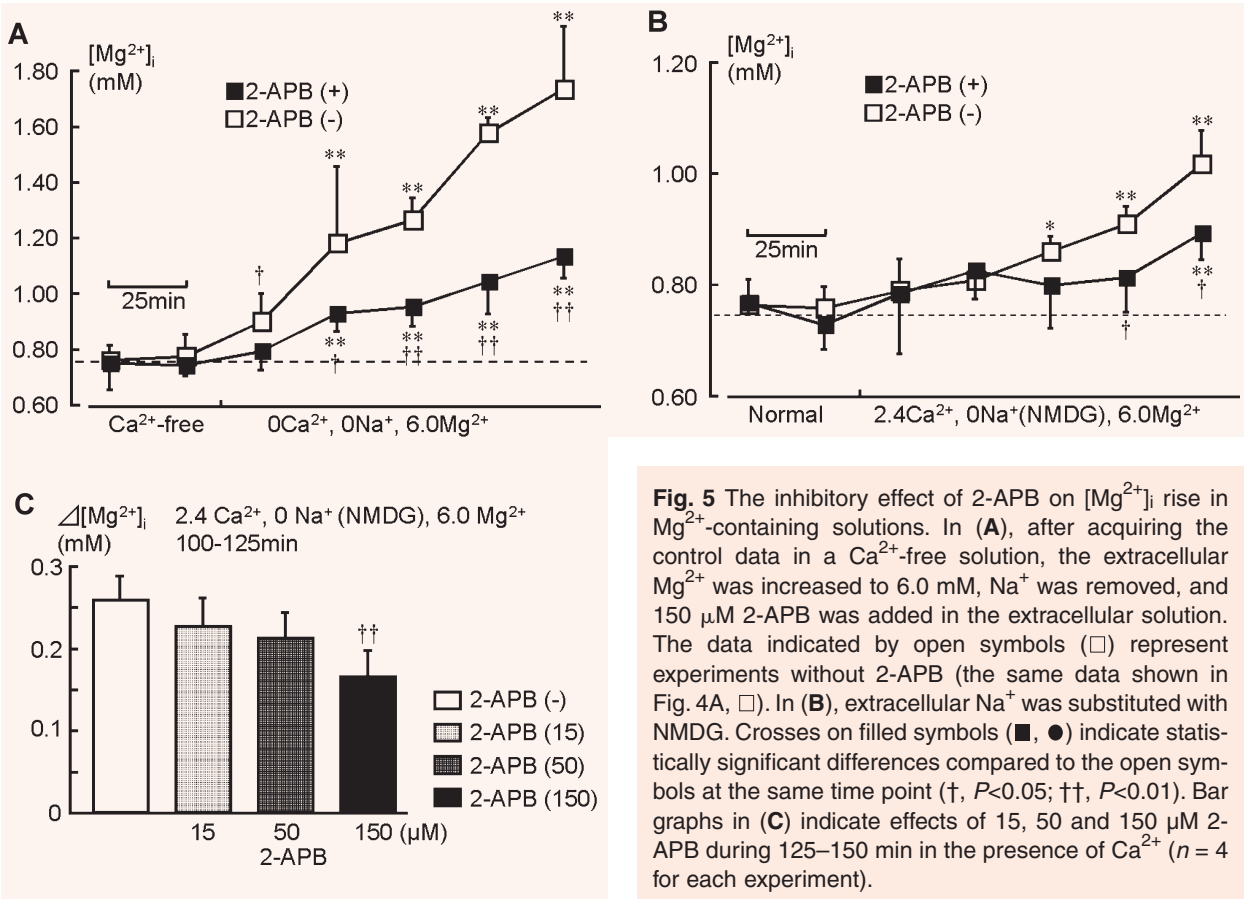


**Fig. 5** The inhibitory effect of 2-APB on $[Mg^{2+}]_i$ rise in $Mg^{2+}$-containing solutions. In (**A**), after acquiring the control data in a $Ca^{2+}$-free solution, the extracellular $Mg^{2+}$ was increased to 6.0 mM, $Na^+$ was removed, and 150 μM 2-APB was added in the extracellular solution. The data indicated by open symbols (□) represent experiments without 2-APB (the same data shown in Fig. 4A, □). In (**B**), extracellular $Na^+$ was substituted with NMDG. Crosses on filled symbols (■, ●) indicate statistically significant differences compared to the open symbols at the same time point (†, $P<0.05$; ††, $P<0.01$). Bar graphs in (**C**) indicate effects of 15, 50 and 150 μM 2-APB during 125–150 min in the presence of $Ca^{2+}$ ($n = 4$ for each experiment).

this procedure maintained the negative membrane potential, unlike $Na^+$ substitution with $K^+$, which was used in other experiments. Furthermore, simultaneous removal of extracellular divalent cations, that is, $Ca^{2+}$ and $Mg^{2+}$, did not significantly decrease $[Mg^{2+}]_i$ when extracellular $Na^+$ was substituted with NMDG (data not shown). Therefore, it is considered that, although $Mg^{2+}$ loss can be caused *via* $Mg^{2+}$-permeable channels under extreme conditions, this mechanism mainly contributes to $Mg^{2+}$ uptake under physiological conditions, in which the negative resting membrane potential is preserved (probably several tens of mV).

TRPM6 and TRPM7 are known $Mg^{2+}$-permeable non-selective cation channels. It has been shown that TRPM6 is abundant in the kidney and small intestine, while TRPM7 is expressed ubiquitously in numerous tissues and organs [9, 21, 22]. It is thought that the former and latter are responsible for $Mg^{2+}$ regulation at the organ and cellular levels, respectively. In line with this notion, RT-PCR examinations revealed that TRPM7 was a major component of TRPM homologues in porcine carotid arteries, but TRPM6 was also detectable (Fig. 7). Previous patch clamp studies have shown that the removal of extracellular divalent cations facilitates TRPM7-like current [9, 11, 23], a finding that is in good agreement with our $[Mg^{2+}]_i$ measurements, that is Figure 5.

2-APB is known to block store-operated $Ca^{2+}$ release-activated $Ca^{2+}$ (CRAC) channels as well as $Mg^{2+}$-permeable channels [24]. However, $Mg^{2+}$ transport *via* CRAC channels is considered negligible, because these channels have even greater $Ca^{2+}$ selectivity than voltage-sensitive $Ca^{2+}$ channels [25]. In the present study, $Mg^{2+}$ transport *via* $Mg^{2+}$-permeable channels demonstrated as $Na^+$-independent $[Mg^{2+}]_i$ changes, was not completely suppressed by 2-APB at <150 μM, which is three times greater than the $IC_{50}$ (~50 μM) reported for TRPM7-like cation currents [11, 23]. This discrepancy may be explained as follows: (1) The $IC_{50}$ of 2-APB in TRPM7 may be altered by the intracellular milieu, namely, $[ATP]_i$ is

maintained in our $^{31}$P-NMR measurements, while no ATP was added in the intracellular solution of the previous patch clamp experiments in which the effect of 2-APB was examined [11, 23]; (2) Native TRP channels may act as multimeric proteins of complex compositions [26]; 3) some other, as yet unknown $Mg^{2+}$ transport mechanisms operate in parallel. Recently, it has been shown that the application of 2-APB does not block, but rather facilitates TRPM6 [27], which is contained as a minor component in porcine carotid arteries. In future studies, it would thus be interesting to examine the effects of drugs, such as 2-APB in TRPM6/7 knockdown cells. NMR measurements provide us with abundant information on $[Mg^{2+}]_i$ regulation, that is $pH_i$ and $[ATP]_i$ which affect intracellular $Mg^{2+}$-buffering, but require a considerable amount of vascular smooth muscle tissue to achieve reasonable time-resolution. For tissue level experiments, gene-targeting techniques, for example, RNA interference, remain to be improved.

The TRPM homologue channels consist of channel pore and kinase domains. Thus, these channels are referred to as 'chanzymes'. It has been reported that $Mg^{2+}$ and MgATP regulate the activity of TRPM7 *via* the kinase domain [9–11, 28]. In addition to this mechanism, intracellular ATP itself acts as an important $Mg^{2+}$ buffer. With respect to the inhibitory effect of 2-APB on $[Mg^{2+}]_i$ rise in the absence of extracellular $Ca^{2+}$ and $Na^+$ (in the presence of 6 mM $Mg^{2+}$; Fig. 4), one may suspect that 2-APB interacts with the kinase domain to elevate its sensitivity to $[Mg^{2+}]_i$. If this mechanism operates, increase in $[Mg^{2+}]_i$ would be slowed at around the $[Mg^{2+}]_i$ which significantly reduces the open probability of the $Mg^{2+}$-permeable channels. The present $^{31}$P-NMR measurements, however, revealed that changes in $[Mg^{2+}]_i$ were suppressed throughout the application of 2-APB (Fig. 6; Supplementary Material IV, Supplementary Table S1). Therefore, the present results suggest that 2-APB directly blocks $Mg^{2+}$-permeable channels at the channel pore.

Reported values for $[Mg^{2+}]_i$ in smooth muscle cells are lower than found in the other two muscle types, that is, skeletal and cardiac muscles. Furthermore, among smooth muscles distributed in numerous tissues and organs, we estimated $[Mg^{2+}]_i$ in vascular smooth muscle cells to be the lowest after correcting for the $pH_i$ and temperature [8]: (0.8-0.85 mM in taenia caeci; 0.7–0.9 mM in the uterus; 0.8 mM in the urinary bladder and 0.65–0.75 mM in the carotid

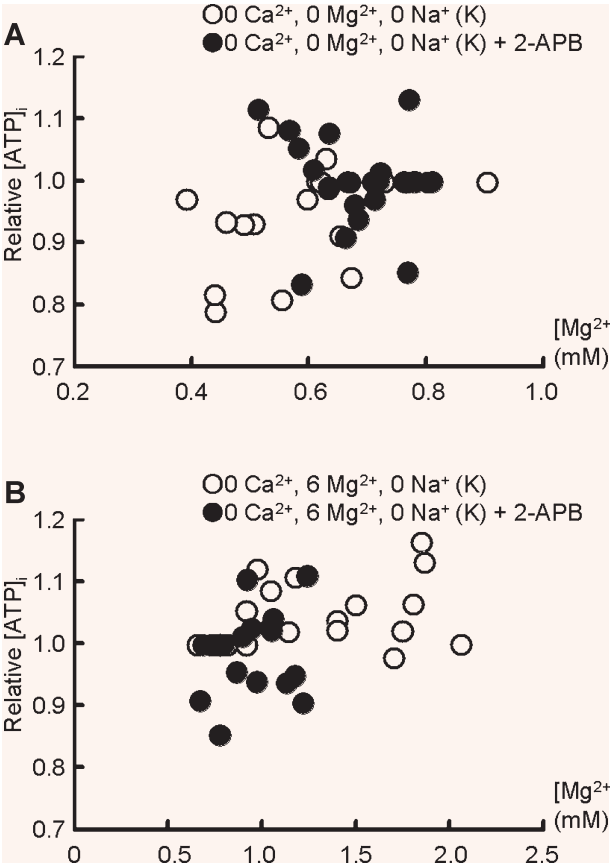


**Fig. 6** Correlation between $[ATP]_i$ and $[Mg^{2+}]_i$ in the absence (0 $Mg^{2+}$; **A**) and presence of extracellular $Mg^{2+}$ (6 mM $Mg^{2+}$; **B**). Each open (○) and filled circle (●) represents a $^{31}$P-NMR data point (spectrum accumulated over 25 min) obtained in the absence and presence of 2-APB, respectively. $[ATP]_i$ is expressed relative to that in the control. Data points in (**A**) are from experiments shown in Fig. 3, while those in (**B**) are from Fig. 5A.

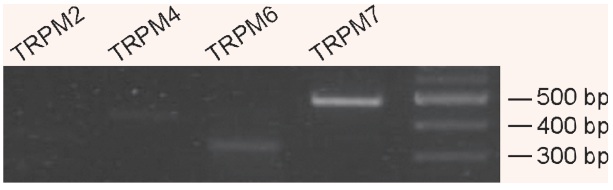


**Fig. 7** RT-PCR detection of TRPM channel members in porcine carotid arteries. The PCR amplification was performed by 35 cycles. A 100-bp molecular weight marker was used (right column). The size of each PCR product is as expected from the mouse and human sequences.

artery. Under divalent cation-free conditions, $[Mg^{2+}]_i$ decreased to ~60% of the control value after 125 min in porcine carotid arteries, however, the decrease in $[Mg^{2+}]_i$ was much slower than that previously observed in intestinal smooth muscle cells (a decrease to tens of μM after 100 min) [6, 17]. The difference in the rate of $[Mg^{2+}]_i$ depletion under $Na^+$-free conditions suggests that the activity of $Mg^{2+}$-permeable channels is lower in vascular smooth muscle cells. This hypothesis may account for the fact that the lowest basal $[Mg^{2+}]_i$ level has been estimated in vascular smooth muscle cells and may contribute to our understanding of $Mg^{2+}$-dependent cellular mechanisms. For example, the physiological significance of $Ca^{2+}$-induced $Ca^{2+}$ release from ryanodine receptors in vascular smooth muscle could be attributed to the low $[Mg^{2+}]_i$ [29]. Also, $Mg^{2+}$-permeable non-selective cation channels, such as TRPM7, have been recently shown to play a crucial role in generating spontaneous rhythmicity in pacemaker interstitial cells of intestinal smooth muscle tissues [30, 31]. Taken together, these facts warrant systematic investigation into cell- and tissue-specific roles of TRPM channels in numerous smooth muscle tissues containing pacemaker-like interstitial cells [32–35].

Functional mutations of ion channels are known to cause numerous diseases. Functional mutations of TRPM7 result in a significant effect on cellular $Mg^{2+}$ homeostasis. It has been experimentally shown that mutations of the kinase domain in TRPM7 modulate the sensitivity to $[Mg^{2+}]_i$. Furthermore, knockout of TRPM7 causes intracellular $Mg^{2+}$-deficiency in cultured cells [36]. In clinical fields, it has long been recognized that $Mg^{2+}$ is associated with several important diseases, *e.g.* diabetes mellitus, hypertension, and cardiovascular and cerebrovascular diseases [37, 38]. Subgroups of these diseases may involve functional mutations of $Mg^{2+}$-permeable channels contributing to passive $Mg^{2+}$ transport *via* the electrochemical gradient. Similarly to the studies on TRPM6 [39, 40], future genetic analyses to clarify the contribution of TRPM7-like $Mg^{2+}$-permeable channels to cardiovascular diseases will be of great interest. Indeed, a TRPM7 variant has been recently reported for two Guamanian neurodegenerative disorders [41].

In conclusion, the present $^{31}$P-NMR data have suggested the existence of $Mg^{2+}$-permeable channels of TRPM homologues, contributing to $[Mg^{2+}]_i$ regulation in vascular smooth muscle cells. The fact that $[Mg^{2+}]_i$ decreases slowly under divalent cation-free conditions, presumably corresponding to the low expression level and/or activity of $Mg^{2+}$-permeable channels, may account for the low basal $[Mg^{2+}]_i$ in vascular smooth muscle cells. From the inhibitory effect of 2-APB and the results of RT-PCR, TRPM7 appears to play a predominant role in the passive $Mg^{2+}$ transport.

## Acknowledgements

The authors are grateful to Dr Lorraine M. Smith (Edinburgh University, U.K.) for useful discussions and improvement in the manuscript, and to Nagoya Meat Hygiene Laboratory (Nagoya, Japan) for continuous supply of porcine carotid arteries.

## Supplementary material

The following supplementary material is available for this article:

**Material S1** Details of estimation procedures.
**Fig. S1** Example spectra for changes in the β-ATP peak during exposures to a $Ca^{2+}$- and $Na^+$-free, high (6.0 mM) $Mg^{2+}$ solution.
**Fig. S2** The effect of amiloride on $[Mg^{2+}]_i$.
**Fig. S3** Tests of primers.
**Table S1** Changes in the concentration of high-energy phosphates.

This material is available as part of the online article from:
http://www.blackwell-synergy.com/doi/abs/10.1111/j.1582-4934.2007.00157.x

(This link will take you to the article abstract).
Please note: Blackwell Publishing are not responsible for the content or functionality of any supplementary materials supplied by the authors. Any queries (other than missing material) should be directed to the corresponding author for the article.

## References

1. **McGuigan JAS, Elder HY, Günzel D, Schlue W-R.** Magnesium homeostasis in heart: a critical reappraisal. *J Clin Basic Cardiol.* 2002; 5: 5–22.

2. **Vaskonen T.** Dietary minerals and modification of cardiovascular risk factors. *J Nutr Biochem.* 2003; 14: 492–506.
3. **Touyz RM.** Magnesium in clinical medicine. *Front Biosci.* 2004; 9. 1278–93.
4. **Kisters K, Tepel M, Spieker C, Zidek W, Barenbrock M, Tokmak F., Kosch M, Hausberg M, Rahn KH.** Decreased membrane $Mg^{2+}$ concentrations in a subgroup of hypertensives: membrane model for the pathogenesis of primary hypertension. *Am J Hypertens.* 1998; 11: 1390–3.
5. **Flatman PW, Smith LM.** Magnesium transport in ferret red cells. *J Physiol.* 1990; 431: 11–25.
6. **Nakayama S, Tomita T.** Regulation of intracellular free magnesium concentration in the taenia isolated from guinea-pig caecum. *J Physiol.* 1991; 435: 559–72.
7. **Handy RD, Gow IF, Ellis D, Flatman PW.** Na-dependent regulation of intracellular free magnesium concentration in isolated rat ventricular myocytes. *J Mol Cell Cardiol.* 1996; 28: 1641–51.
8. **Nakayama S, Clark JF.** Smooth muscle and NMR review: An overview of smooth muscle metabolism. *Mol Cell Biochem.* 2003; 244: 17–30.
9. **Nadler MJS, Hermosura MC, Inabe K, Perraud AL, Zhu Q, Strokes AJ, Kurosaki T, Kinet JP, Penner R, Scharenberg AM, Fleig A.** LTRPC7 is a Mg.ATP-regulated divalent cation channel required for cell viability. *Nature.* 2001; 411: 590–5.
10. **Runnels LW, Yue L, Clapham DE.** TRP-PLIK, a bifunctional protein with kinase and ion channel activities. *Science.* 2001; 291: 1043–7.
11. **Hermosura MC, Monteilh-Zoller MK, Scharenberg AM, Penner R, Fleig A.** Dissociation of the store-operated calcium current I(CRAC) and the Mg-nucleotide-regulated metal ion current MagNuM. *J Physiol.* 2002; 539: 445–58.
12. **Uetani T, Matsubara T, Nomura H, Murohara T, Nakayama S.** $Ca^{2+}$-dependent modulation of intracellular $Mg^{2+}$ concentration with amiloride and KB-R7943 in pig carotid artery. *J Biol Chem.* 2003; 278: 47491–7.
13. **Dillon PF.** $^{31}P$ Nuclear magnetic resonance spectroscopy. In: Bárány M, editors. Biochemistry of Smooth Muscle Contraction. San Diego: Academic Press; 1996. pp. 393–404.
14. **Kushmerick MJ, Dillon PF, Meyer RA, Brown TR, Krisanda JM, Sweeney HL.** $^{31}P$ NMR spectroscopy, chemical analysis, and free $Mg^{2+}$ of rabbit bladder and uterine smooth muscle. *J Biol Chem.* 1986; 261: 14420–9.
15. **Nakayama S, Nomura H, Smith LM, Clark JF.** Simultaneous estimation of intracellular free $Mg^{2+}$ and pH using a new pH-dependent dissociation constant of MgATP. *Jpn J Physiol.* 2002; 52: 323–6.
16. **Zhang W, Truttmann AC, Lüthi D, McGuigan JAS.** Apparent $Mg^{2+}$-adenosine 5′-triphosphate dissociation constant measured with $Mg^{2+}$ macroelectrodes under conditions pertinent $^{31}P$-NMR ionized magnesium determinations. *Anal Biochem.* 1997; 251: 246–50.
17. **Nakayama S, Nomura H, Smith LM, Clark JF, Uetani T, Matsubara T.** Mechanisms for monovalent cation-dependent depletion of intracellular $Mg^{2+}$: $Na^{+}$-independent $Mg^{2+}$ pathways in guinea-pig smooth muscle. *J Physiol.* 2003; 551: 843–53.
18. **Kajioka S, Nakayama S, Asano H, Brading AF.** Involvement of ryanodine receptors in muscarinic-receptor-mediated membrane current oscillation in urinary bladder smooth muscle. *Am J Physiol.* 2005; 288: C100–8.
19. **Simchrowitz L, Kleyman TR, Cragoe Jr EJ.** An overview of the structure-activity relations in the amiloride series. In: Cragoe Jr EJ, Kleyman TR, Simchowitz L, editors. Amiloride and Its Analogues. New York: VCH Publishers; 1992. pp. 9–24.
20. **Nakayama S, Nomura H.** Mechanisms of intracellular $Mg^{2+}$ regulation affected by amiloride and ouabain in the guinea-pig taenia caeci. *J Physiol.* 1995; 488: 1–12.
21. **Voets T, Nilius B, Hoefs S, van der Kemp AW, Droogmans G, Bindels RJ, Hoenderop JG.** TRPM6 forms the $Mg^{2+}$ influx channel involved in intestinal and renal $Mg^{2+}$ absorption. *J Biol Chem.* 2004; 279: 19–25.
22. **Montell C.** $Mg^{2+}$ homeostasis: the $Mg^{2+}$ nificent TRPM chanzymes. *Curr Biol.* 2003; 13: R799–801.
23. **Prakriya M, Lewis RS.** Separation and characterization of currents through store-operated CRAC channels and $Mg^{2+}$-inhibited cation (MIC) channels. *J Gen Physiol.* 2002; 119: 487–507.
24. **Bootman MD, Collins TJ, Mackenzie H, Roderick HL, Berridge MJ, Peppiatt CM.** 2-Aminoethoxydiphenyl borate (2-APB) is a reliable blocker of store-operated $Ca^{2+}$ entry but an inconsistent inhibitor of InsP3-induced $Ca^{2+}$ release *FASEB J.* 2002; 16: 1145–50.
25. **Parekh AB, Putney Jr JW.** Store-operated calcium channels. *Physiol Rev.* 2005; 85: 757–810.
26. **Schaefer M.** Homo- and heteromeric assembly of TRP channel subunits. *Pflügers Arch.* 2005; 451: 35–42.
27. **Li M, Jiang J, Yue L.** Functional characterization of homo- and heteromeric channel kinases TRPM6 and TRPM7. *J Gen Physiol.* 2006; 127: 525–37.
28. **Demeuse P, Penner R, Fleig A.** TRPM7 channel is regulated by magnesium nucleotides *via* its kinase domain. *J Gen Physiol.* 2006; 127: 421–34.
29. **Ogawa Y, Murayama T, Kurebayashi N.** Ryanodine receptor isoforms of non-mammalian skeletal muscle. *Front Biosci.* 2002; 7: d1187–94.

30. **Kim BJ, Lim HH, Yang DK, Jun JY, Chang IY, Park CS, So I, Stanfield PR, Kim KW.** Melastatin-type transient receptor potential channel 7 is required for intestinal pacemaking activity. *Gastroenterol.* 2005; 129: 1504–17.
31. **Nakayama S, Kajioka S, Goto K, Takaki M, Liu H-N.** Calcium-associated mechanisms in gut pacemaker activity. *J Cell Mol Med.* 2007; 11: 958–68.
32. **Huizinga JD, Faussome-Pellegrini MS.** About the presence of interstitial cells of Cajal outside the musculature of the gastrointestinal tract. *J Cell Mol Med.* 2005; 9: 468–73.
33. **Harhun MI, Pucovsky V, Povstyan OV, Gordienko DV, Bolton TB.** Interstitial cells in the vasculature. *J Cell Mol Med.* 2005; 9: 232–43.
34. **Popescu LM, Ciontea SM, Cretoiu D.** Interstitial Cajal-like cells in human uterus and fallopian tube. *Ann N Y Acad Sci.* 2007; 1101: 139–65.
35. **Brading AF, McCloskey KD.** Mechanisms of Disease: specialized interstitial cells of the urinary tract—an assessment of current knowledge. *Nat Clin Pract Urol.* 2005; 2: 546–54.
36. **Schmitz C, Perraud AL, Johnson CO, Inabe K, Smith MK, Penner R, Kurosaki T, Fleig A, Scharenberg AM.** Regulation of vertebrate cellular $Mg^{2+}$ homeostasis by TRPM7. *Cell.* 2003; 114: 191–200.
37. **Paolisso G, Barbagallo M.** Hypertension, diabetes mellitus, and insulin resistance: the role of intracellular magnesium. *Am J Hypertens.* 1997; 10: 368–70.
38. **Yang C-Y.** Calcium and magnesium in drinking water and risk of death from cerebrovascular disease. *Stroke.* 1998; 29: 411–4.
39. **Schlingmann KP, Weber S, Peters M, Niemann Nejsum L, Vitzthum H, Klingel K, Kratz M, Haddad E, Ristoff E, Dinour D, Syrrou M, Nielsen S, Sassen M, Waldegger S, Seyberth HW, Konrad M.** Hypomagnesemia with secondary hypocalcemia is caused by mutations in TRPM6, a new member of the TRPM gene family. *Nat Genet.* 2002; 31: 166–70.
40. **Walder RY, Landau D, Meyer P, Shalev H, Tsolia M, Borochowitz Z, Boettger MB, Beck GE, Englehardt RK, Carmi R, Sheffield VC.** Mutation of TRPM6 causes familial hypomagnesemia with secondary hypocalcemia. *Nat Genet.* 2002; 31: 171–4.
41. **Hermosura MC, Nayakanti H, Dorovkov MV, Calderon FR, Ryazanov AG, Haymer DS, Garruto RM.** A TRPM7 variant shows altered sensitivity to magnesium that may contribute to the pathogenesis of two Guamanian neurodegenerative disorders. *Proc Natl Acad Sci USA.* 2005; 102: 1510–5.